Electrochimica Acta 271 (2018) 498–506

Contents lists available at ScienceDirect

Electrochimica Acta

journal homepage: www.elsevier.com/locate/electacta

Effect of reaction temperature on the amorphous-crystalline transition of copper cobalt sulfide for supercapacitors

SongHao Guo [a, b], WenQiang Chen [a], M. Li [a, c], Jun Wang [d], F. Liu [a], J.P. Cheng [a, *]

[a] State Key Laboratory of Silicon Materials, School of Materials Science and Engineering, Key Laboratory of Advanced Materials and Applications for Batteries of Zhejiang Province, Zhejiang University, Hangzhou, 310027, China
[b] Center for High Pressure Science and Technology Advanced Research (HPSTAR), Shanghai, 201203, China
[c] Research Institute of Narada Power Source Co., Ltd, Hangzhou, 311305, China
[d] School of Physical Science and Technology, Lanzhou University, Lanzhou, 730000, China

HPSTAR 582-2018

ARTICLE INFO

Article history:
Received 7 February 2018
Received in revised form
26 March 2018
Accepted 29 March 2018
Available online 31 March 2018

Keywords:
Copper cobalt sulfide
Amorphous-crystalline transition
Hydrothermal temperature
Supercapacitor

ABSTRACT

Amorphous and crystalline copper cobalt sulfides are successfully synthesized *via* a hydrothermal method at different temperatures and researched as electrode materials for supercapacitor. The reaction mechanisms during the sulfidation and hydrothermal processes are investigated and clarified. It is demonstrated that the hydrothermal temperature is a crucial factor for the crystallinity, morphology and electrochemical performance of $CuCo_2S_4$. Among all the samples, the $CuCo_2S_4$ synthesized at 150 °C shows the highest specific capacitance of 515 F g^{-1} at 1 A g^{-1} as well as good cycling stability with ~93.3% capacitance retention after 10000 cycles at 5 A g^{-1}. An asymmetric device which is assembled by using optimized $CuCo_2S_4$ electrode as positive electrode and activated carbon as negative electrode material is able to deliver an ultrahigh energy density of 50.56 Wh kg^{-1} at a power density of 4.6 kW kg^{-1}, and remains 20.93 Wh kg^{-1} at a high power density of 22.5 kW kg^{-1}, with ~99% capacity retention after 10000 cycles. Based on the results above, the $CuCo_2S_4$ materials prepared by our method possess a considerable potential as electrode materials for supercapacitor applications.

1. Introduction

Electrochemical capacitors (ECs), also known as supercapacitors (SCs), are new energy storage devices which have attracted much research interest and have been widely used in portable electronics and electric vehicles [1–5]. They have gradually become an alternative option of batteries gradually due to their unique advantages, *i.e.* fast charge and discharge process [6], excellent cycling stability [7] and facile productive process [8]. In general, the electrochemical performances of ECs are strongly dominated by electrode materials, such as carbon materials [9], transition metal compounds [10,11] and conductive polymers [12].

In recent years, transition metal oxides and hydroxides have been widely investigated as electrode materials for ECs because of their higher energy density than that of carbon materials [13,14]. Nevertheless, the poor cycling stability, low electrical conductivity and limited power density have restrained their potential applications in energy storage [14–17]. Due to the lower electronegativity of sulfur than that of oxygen, transition metal sulfides possess higher electroconductivity and more effective electrochemical activity compared with metal oxides and hydroxides, which can thus provide faster transport pathways for electrons [18]. Furthermore, binary-metal sulfides can exhibit better electrochemical properties than single-metal sulfides owing to abundant redox reactions and the synergistic effect between two metal elements [19–22].

Recently, copper cobalt sulfide ($CuCo_2S_4$) has been investigated as an active electrode material with a relatively high energy density for ECs. For example, Zhang et al. prepared flower-like $CuCo_2S_4$ nanosheet arrays directly grown on Ni foam which exhibited a high specific capacitance of 908.9 F g^{-1} at 5 mA cm^{-2} [23]. Wang et al. successfully fabricated $CuCo_2S_4$ with uniform flower-like structure *via* a traditional two-step hydrothermal method, and it was able to deliver a specific capacitance of 592 F g^{-1} at 1 A g^{-1} and 518 F g^{-1} at 10 A g^{-1} [24]. Moosavifard et al. synthesized hierarchical $CuCo_2S_4$ hollow nanoneedle arrays on Ni foam which was applied as binder-free electrodes with a high specific capacitance of 2163 F g^{-1} at 6 mA cm^{-2} [25]. Wang et al. directly prepared oriented $CuCo_2S_4$

* Corresponding author.
E-mail address: chengjp@zju.edu.cn (J.P. Cheng).

https://doi.org/10.1016/j.electacta.2018.03.189
0013-4686/

nanograss arrays on Ni foam and achieved a high energy density of 31.88 Wh kg^{-1} at a power density of 3.20 kW kg^{-1} [26]. The $CuCo_2S_4$ materials reported in all above literature were synthesized by a two-step hydrothermal method using sodium sulphide as the sulfur source and the resultant $CuCo_2S_4$ products were mostly deposited on metal substrates.

In our previous work, we successfully synthesized Cu-Co carbonate hydroxide microspheres as a battery-like electrode material *via* a one-step hydrothermal method [27], which possessed a unique dandelion-like structure and exhibited excellent cycling stability. Meanwhile, we also found that when the brown Cu-Co carbonate hydroxide met saturated Na_2S solution at room temperature, it would form a metal sulfide product and turn black rapidly. The XRD analyses revealed that the black product was amorphous and it could be crystallized by subsequent hydrothermal treatment. Though there are many reports focused on the electrochemical performance of $CuCo_2S_4$ materials [23–26], the influences of the crystallinity on the electrochemical performances of $CuCo_2S_4$ materials have rarely been investigated to the best of our knowledge.

In this work, amorphous and crystalline $CuCo_2S_4$ microspheres could be successfully synthesized *via* a hydrothermal method using Cu-Co carbonate hydroxide as the precursor by controlling the reaction temperature. The $CuCo_2S_4$ would undergo a transformation from amorphous to crystalline during the sulfidation and hydrothermal process above 100 °C. We found that the reaction temperature was a key factor to the crystallinity of $CuCo_2S_4$ which would dominate the electrochemical performances, and the $CuCo_2S_4$ hydrothermally synthesized at 150 °C was able to obtain the highest specific capacitance of 515 F g^{-1} at a current density of 1 A g^{-1} with a good cycling stability. An asymmetric supercapacitor (ASC) which was fabricated by using optimized $CuCo_2S_4$ electrode as positive electrode and activated carbon (AC) as negative electrode exhibited an ultrahigh energy density of 50.56 Wh kg^{-1} at a power density of 4.6 kW kg^{-1} and an excellent cycling stability with ~99% capacity retention after 10000 cycles at 5 A g^{-1}.

2. Experimental

2.1. Synthesis of $CuCo_2S_4$ materials

The precursor *i.e.* Cu-Co carbonate hydroxide with the Cu to Co molar ratio of 1:2 was synthesized by a hydrothermal method as reported previously [27]. Then $CuCo_2S_4$ materials were synthesized as the following process. 0.2 g precursor was dispersed in 50 ml water under stirring, then 20 ml saturated Na_2S solution was dropwise added into the suspension of the precursor at room temperature. After the color of the suspension turned into black, the suspension was transferred into a 100 ml Teflon-lined stainless autoclave and kept at room temperature, 100 °C, 150 °C and 200 °C for 4 h to allow the growth of $CuCo_2S_4$ materials with the name of CCS-RT, CCS-100, CCS-150 and CCS-200, respectively. After reaction, the resultant product was filtrated and fully washed by deionized water and ethanol, then dried at 80 °C for 8 h.

2.2. Preparation of electrode

The electrodes were prepared according to the following steps. After dispersing the mixture of 80 wt% of $CuCo_2S_4$, 10 wt% of acetylene black and 10 wt% of PVDF in some 1-methyl-2-pyrrolidone, the homogeneous slurry formed was coated onto a piece of Ni foam (1.5 cm × 1.5 cm) as a current collector. Then the electrodes were dried at 80 °C for 10 h before electrochemical measurement. The mass loading of electrode materials on each electrode was approximately 5 mg.

2.3. Materials characterization

The phase and crystal structure of $CuCo_2S_4$ were characterized by a powder X-ray diffractometer (Shimadzu, XRD-6000) using Cu-Kα irradiation (λ = 1.5406 Å) from 10° to 80° with the scanning rate of 3° min^{-1}. A scanning electron microscope (SEM, Hitachi S-4800) and a transmission electron microscope (TEM, Philips-CM200) were used to characterize their morphology and microstructure. The chemical analyses of the sample were measured by X-ray photoelectron spectroscopy (XPS, Shimadzu, AXIS Supra). Fourier transformed infrared (FTIR) spectrum was measured by Bruker spectrometer (TENSOR27).

2.4. Electrochemical measurements

The electrochemical performances of electrode materials were measured with a standard three-electrode system in 2 M KOH aqueous solution. The as-prepared electrode, nickel foil and Ag/AgCl electrode were used as working electrode, counter electrode and reference electrode, respectively. Cyclic voltammograms (CV), galvanostatic charge/discharge curves and electrochemical impedance spectrum (EIS) were measured by a CHI660E electrochemical workstation within the frequency range from 100 kHz to 0.01 Hz. The cycling stability was tested in LAND CT2001A test system by galvanostatic charge/discharge processes. The specific capacitance (Cs) of the sample was calculated according to the following equation,

$$C_s = I \cdot \Delta t / (m \cdot \Delta V) \quad (1)$$

where I (A), Δt (s), m (g) and ΔV (V) represent the discharge current, discharge time, mass of active material and potential window, respectively.

Asymmetric devices, *i.e.* $CuCo_2S_4$//AC capacitor, were assembled by using optimized sample CCS-150 as positive electrode, AC as negative electrode, 2 M KOH as electrolyte and a piece of cellulose paper as the separator. Fig. S1 shows the CV curves and galvanostatic charge and discharge curves of AC we used here. The mass ratio of $CuCo_2S_4$ to AC was determined to be 1.12, which was calculated by the charge balance theory [28]. The performances of the hybrid capacitor were measured under a two-electrode system. The energy density (*E*) and power density (*P*) of the asymmetric device can be calculated according to the following equations.

$$E = \frac{1}{2} \cdot C \cdot \Delta V^2 \quad (2)$$

$$P = E / \Delta t \quad (3)$$

where C (F g^{-1}), ΔV (V), Δt (s) represent the specific capacitance of hybrid capacitor, potential window and discharge time, respectively.

3. Results and discussions

3.1. Crystal structure and morphology analyses

The crystal structures of as-synthesized $CuCo_2S_4$ materials were examined by X-ray diffraction (XRD). As shown in Fig. 1, The diffraction peaks for sample CCS-100, CCS-150 and CCS-200 at 2θ = 31.30°, 37.95° and 54.78° are well indexed to the reflection of (113), (004) and (044) planes of crystalline $CuCo_2S_4$ (PDF#42-1450), respectively. However, it is obvious that the $CuCo_2S_4$ material prepared at room temperature (sample CCS-RT) shows a typical amorphous structure, without any refection peaks in the pattern,

which will be also verified by the following TEM observation. There is a tendency that the intensity of the diffraction peaks in XRD patterns increase with the rising hydrothermal temperature, which indicates that the crystallinity of $CuCo_2S_4$ has increased in the hydrothermal process. For comparison, the data of diffraction peaks are listed in Table 1 in detail.

The morphology and microstructure of $CuCo_2S_4$ products were investigated by SEM. Fig. 2 shows the SEM images of all samples under different magnifications. All samples show a morphology of spherical clusters containing numerous nanorods, and there are no obvious changes in terms of morphology comparing with Cu-Co precursors in our previous work [27]. Significantly, sample CCS-200 shows the coexistence of nanorods and nanoplates in Fig. 2(g and h), which indicates that the nanorods will self-assemble into nanoplates during the hydrothermal process when the reaction temperature is as high as 200 °C. However, the XRD diffraction peaks of CCS-200 are also well assigned to the standard pattern of $CuCo_2S_4$, demonstrating that the nanorods and nanoplates have the same crystal structure. It has been confirmed by other reports that nanorods have larger surface area compared to nanoplates, which can possess more effective electrochemical active sites and offer abundant diffusion channels [29,30].

TEM observation was used to further investigate the transformation of $CuCo_2S_4$ from amorphous to crystalline. Fig. 3(a and b) illustrate the separated nanorods of sample CCS-RT under different magnifications. Selected area electron diffraction (SAED) pattern of the nanorods in the inset of Fig. 3a confirms that they are amorphous in nature, which is in good agreement with the results by XRD. Fig. 3(c and d) show an individual nanorod of sample CCS-150. The nanorod shows an obvious porous structure which may be caused by volume expansion in the sulfidation process. A typical SAED pattern in the inset of Fig. 3c confirms the crystalline nature of the nanorod with marked <222> planes. In a high-resolution TEM image in Fig. 3d, the nanorod shows a lattice spacing of 0.57 nm which can be attributed to the (111) plane of the $CuCo_2S_4$ phase. Meanwhile, we can confirm that the nanorod in Fig. 3d is composed of many small single-crystalline nanograins from the clear random lattice fringes. Fig. S2(a) shows the TEM image of sample CCS-200 which is composed of nanorods and nanoplates. The SEAD pattern of CCS-200 in Fig. S2(b) are similar to that of CCS-150, which further confirms that the nanorods and nanoplates are of the same crystal structure.

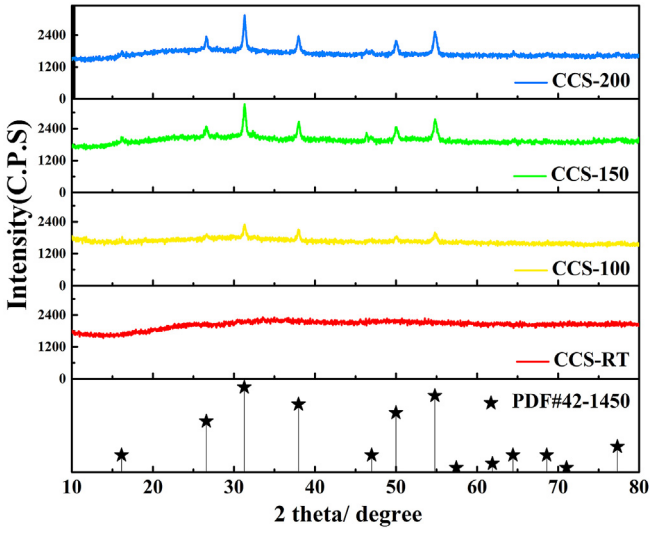

Fig. 1. XRD patterns of all the samples under different hydrothermal temperatures and the standard pattern of CuCo2S4 (PDF No.42-1450).

Table 1
The data of diffraction peaks.

Sample	(hkl)	Intensity (C.P.S)	Integral area (a.u.)
CCS-100	(113)	498	18461
	(044)	373	21193
CCS-150	(113)	1169	49341
	(044)	795	42975
CCS-200	(113)	1303	54001
	(044)	869	50611

FTIR spectra of all the samples are presented in Fig. S3. From the spectra, we can easily draw a conclusion that they are of the same vibration between metal and sulfur, which are close to the previous report [31].

Based on the above results, it is confirmed that even at room temperature, $CuCo_2S_4$ material can be also easily synthesized through a simple sulfidation process. The crystalline Cu-Co carbonate hydroxide precursor will go through a precipitation conversion reaction in Na_2S solution due to the lower solubility constant of metal sulfides than that of metal carbonate hydroxides [32]. The mechanisms of the reaction are as follows.

$$(Cu,Co)_2(CO_3)(OH)_2 \rightleftarrows 2Co^{2+} + Cu^{2+} + CO_3^{2-} + 2OH^- \quad (4)$$

$$2Co^{2+} + Cu^{2+} + 4S^{2-} \rightleftarrows CuCo_2S_4 \quad (5)$$

The $CuCo_2S_4$ synthesized at room temperature will form an amorphous structure owing to the different lattice constants of crystalline $CuCo_2S_4$ and $(Cu,Co)_2(CO_3)(OH)_2$ which also caused the volume expansion. Because of the higher Gibbs free energy of amorphous materials than that of crystalline materials, the amorphous $CuCo_2S_4$ would crystalize by hydrothermal treatment spontaneously. As we all know, the reaction velocity can be strongly dominated by the reaction temperature according to Arrhenius equation [33]. Thus, the reaction temperature is a key factor to the crystallinity of $CuCo_2S_4$ materials.

Chemical composition and states of sample CCS-150 were investigated by XPS analysis, as shown in Fig. 4. Each peak can be assigned correctly in the wide spectrum in Fig. 4a, which confirms a high purity of the sample. The high-resolution spectrum for S 2p in Fig. 4b reveals two peaks at 162.7 eV and 161.5 eV, which are assigned to S $2p_{1/2}$ and S $2p_{3/2}$ species, respectively. In the Cu 2p high-resolution XPS spectrum (Fig. 4c), the Cu 2p deconvoluted spin–orbit peaks display $2p_{3/2}$ electronic configurations at 932.5 eV and 934.2 eV, signifying the di-valent and tri-valent states of Cu, respectively. The spin–orbit peaks at 952.2 eV and 953.2 eV correspond to the Cu $2p_{1/2}$ electronic configurations. Fig. 4d exhibits Co 2p XPS spectrum, where two peaks at 779.1 eV and 794.3 eV are corresponding to Co $2p_{3/2}$ and Co $2p_{1/2}$ signals of Co^{3+}, respectively.

3.2. Electrochemical properties

The electrochemical properties of the $CuCo_2S_4$ materials synthesized at different temperatures were investigated as ECs electrodes, and their CV curves under different scan rates are shown in Fig. S4. Fig. 5a shows the CV curves of all the samples at a scan rate of 5 mV s^{-1} from 0 to 0.55 V. An anodic peak at 0.05 V and a cathodic peak at 0.33 V are derived from the oxidation of Co^{2+} to Co^{3+} and its reverse process [34,35], respectively, whereas another anodic peak at 0.37 V and cathodic peak at 0.20 V are assigned to the oxidation of Cu^{2+} to Cu^{3+} and its reverse process [16,36], respectively. The Faradic redox reactions of $CuCo_2S_4$ can be

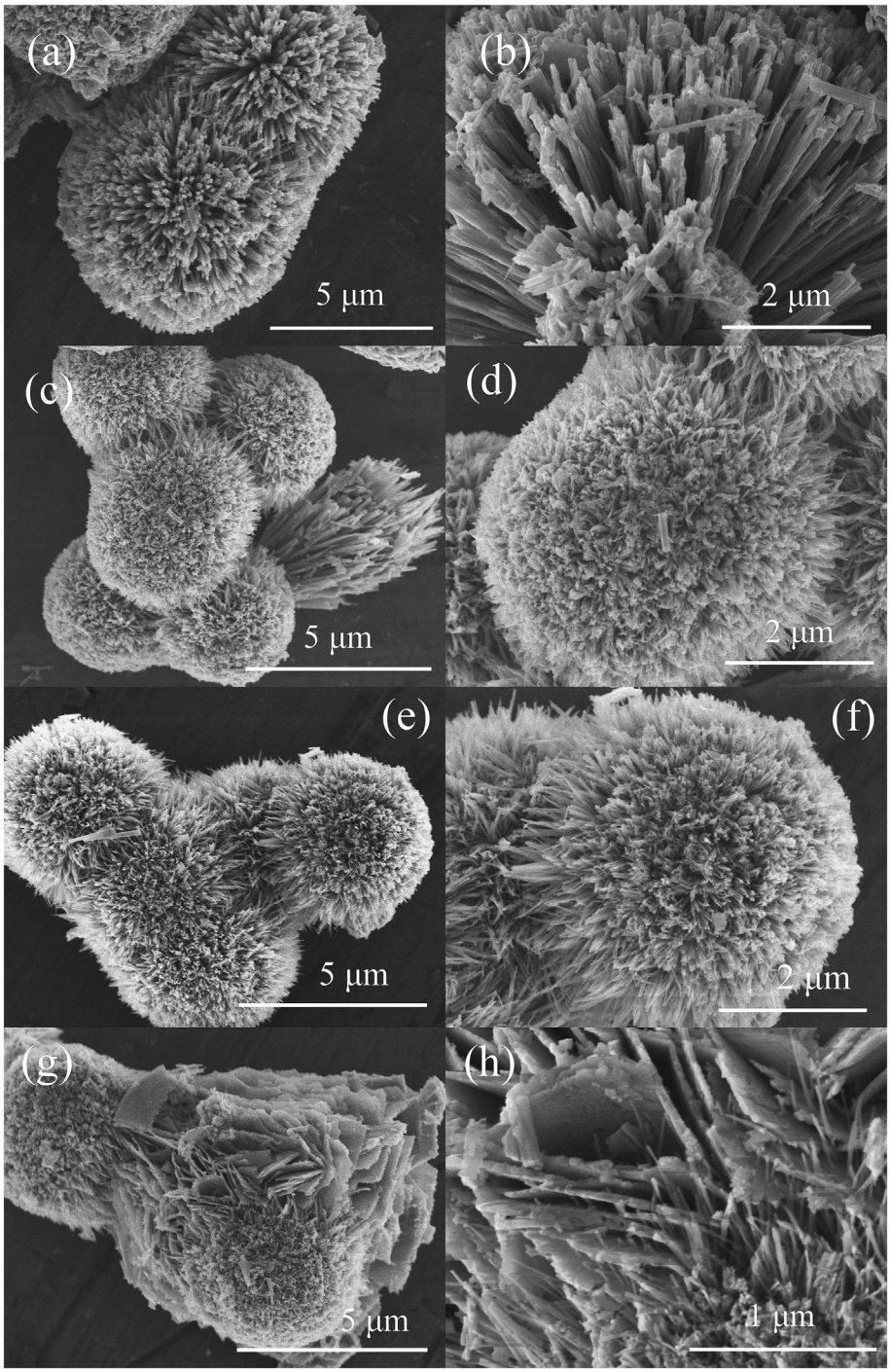

Fig. 2. SEM images of $CuCo_2S_4$ materials under different magnifications, (a,b) CCS-RT, (c,d) CCS-100, (e,f) CCS-150, (g,h) CCS-200.

generally concluded as follows [37],

$$CoS + OH^- \leftrightarrow CoSOH + H_2O + e^- \quad (6)$$

$$CuS + OH^- \leftrightarrow CuSOH + H_2O + e^- \quad (7)$$

It can be noticed that the amorphous sample CCS-RT has a similar CV curve with other crystalline samples, which indicates that the amorphous $CuCo_2S_4$ has the same Faradic reactions as the crystalline $CuCo_2S_4$. From the enclosed area of each curve under the same scan rate, we can generally draw a conclusion that sample CCS-150 has the highest specific capacitance among all the samples. Fig. 5b shows the CV curves of as-prepared CCS-150 electrode with various scan rates of 5, 10, 20, 30 and 50 mV s^{-1}, showing a battery-like performance. The deviation of the redox reaction peak with the increasing scan rate is related to the inner resistance of the electrode itself [38].

The galvanostatic charge and discharge curves of all the samples at 1 A g^{-1} are illustrated in Fig. 6a and those under various current densities are shown in Fig. S5. The specific capacitances for sample CCS-RT, CCS-100, CCS-150 and CCS-200 are calculated to be 281.9, 449.5, 515.0 and 465.7 F g^{-1} at 1 A g^{-1} from the corresponding

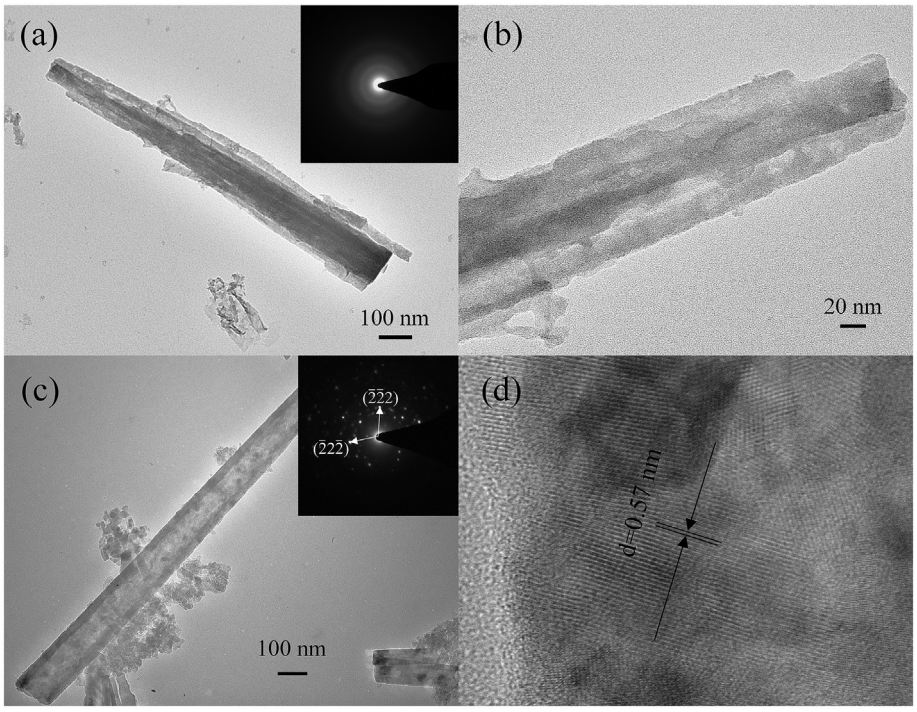

Fig. 3. TEM images and SEAD patterns of $CuCo_2S_4$ materials, (a,b) CCS-RT and (c,d) CCS-150.

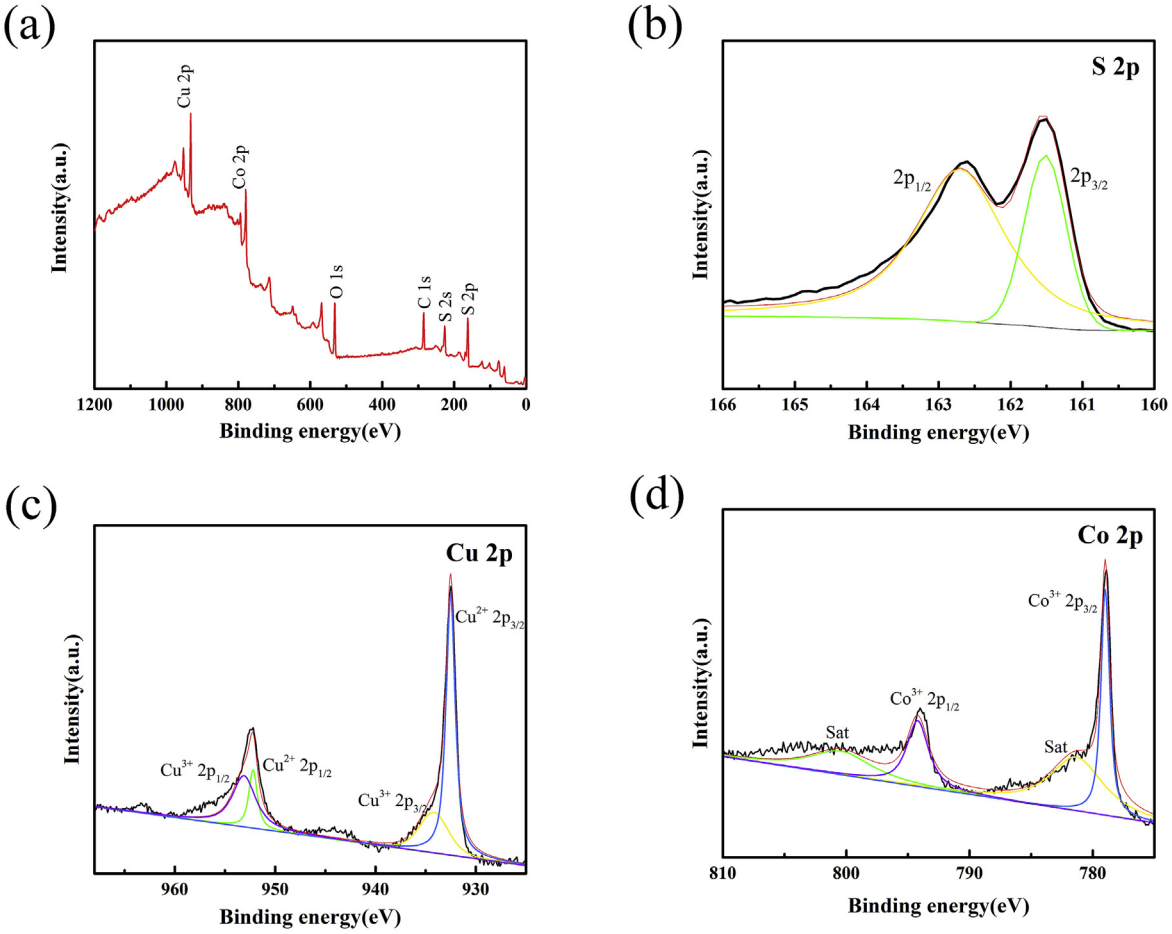

Fig. 4. XPS spectra of sample CCS-150 (a) wide, (b) S 2p, (c) Cu 2p and (d) Co 2p.

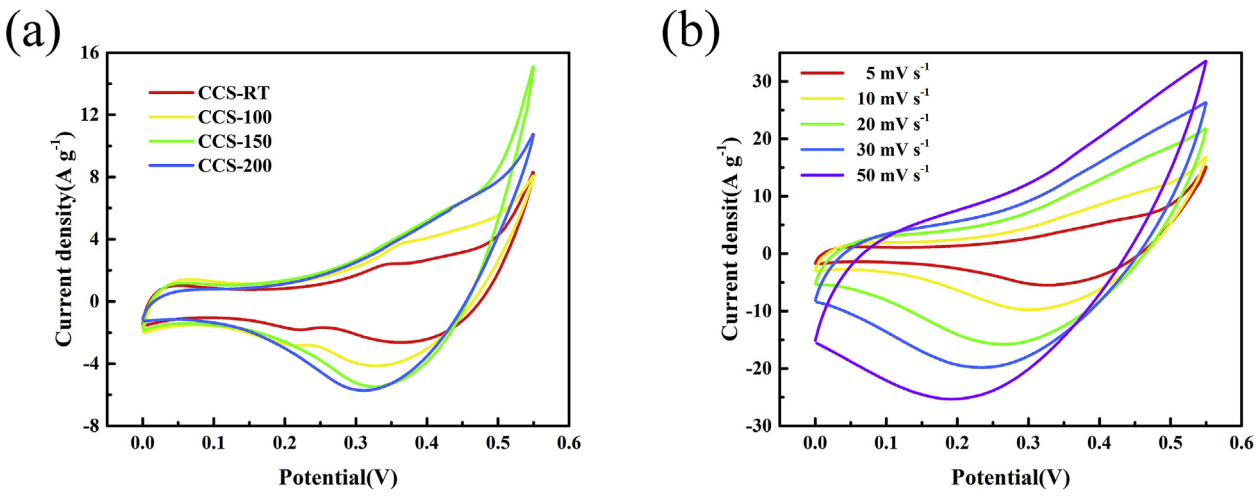

Fig. 5. CV curves of (a) $CuCo_2S_4$ electrode materials at the scan rate of 5 mV s^{-1}, (b) CCS-150 electrode at various scan rates.

discharge curves, respectively. We can see that the specific capacitance increases initially with the increase of hydrothermal temperature, which indicates that enhanced electrochemical performances can be obtained by increasing the crystallinity of the $CuCo_2S_4$ materials. In general, electrode materials with a high crystallinity will have a high conductivity and good structural stability, which are two important features for an ideal electrode material [39]. There will be fewer grain boundaries, resulting in less scattering during electron transport [40]. However, sample CCS-200 shows an abnormal decrease in specific capacitance which may ascribe to the self-assembled behavior during hydrothermal process at a high temperature. The nanorods have a larger surface area than nanoplates, thus more electrochemical active sites and larger contact area of electrode and electrolyte can be obtained in microspheres composed by nanorods [29,30].

Fig. 6b illustrates the galvanostatic charge and discharge curves of sample CCS-150 at 1, 2, 3, 4, 5, 8 and 10 A g^{-1}. Fig. 6c shows the specific capacitance of all the samples as a function of current density. Meanwhile, sample CCS-150 shows the highest specific capacitance at all current densities among them. Though the highest specific capacitance here is lower than the reported values in Refs. [23] [25], and is close to that in Ref. [24], it may ascribe to the fact that all these $CuCo_2S_4$ materials [23–25] are thin films grown on a conductive substrate such as Ni foam or Ti wire. The "dead surface" of electrode materials from the contact with the electrolyte to participate in the Faradaic reactions can be avoided compared with the conventional slurry coating process [39], thus leading to a high specific capacitance, but it is difficult to investigate the reaction mechanisms during sulfidation and hydrothermal process under the interference of substrate.

Electrochemical impedance spectroscopy (EIS) measurements were carried out to further examine the electrochemical behavior of $CuCo_2S_4$ materials at the potential of 5 mV in the frequency range from 100 kHz to 0.01 Hz, as shown in Fig. 6d. The Nyquist plots of the $CuCo_2S_4$ electrodes consist of a partial semicircle in the high-frequency region and a straight line in the low-frequency region. The straight line and semicircle represent the redox behavior and charge transfer resistance (Rct) of the material [41], respectively. Impressively, all the $CuCo_2S_4$ electrodes exhibit relatively low Rct values (~0.4 Ω), demonstrating that the $CuCo_2S_4$ materials have fast electron transfer properties on the electrode/electrolyte interface due to its unique microstructure and high conductivity [42]. Cycling stability is an important factor for practical supercapacitor applications [43]. Sample CCS-150 was subjected to galvanostatic charge and discharge processes for 10000 cycles at a current density of 5 A g^{-1}. As shown in Fig. 6e, it shows a good cycling stability with ~93.3% of initial specific capacitance retention after 10000 cycles and a high Coulombic efficiency, which proves that the as-synthesized $CuCo_2S_4$ materials have a good stability in both structure and electrochemical performance.

Compared with other samples, sample CCS-150 exhibited relatively better electrochemical properties. In order to further explore the performances of $CuCo_2S_4$ materials for practical applications, we assembled $CuCo_2S_4$//AC ASC devices. Fig. 7a shows the comparative CV curves of both positive and negative electrode materials which are measured in the three-electrode system at a scan rate of 5 mV s^{-1}, suggesting that the as-fabricated ASC device will have a stable operating voltage for at least 1.6 V. Therefore, a potential window of 1.6 V is selected herein to investigate the electrochemical properties of the ASC device, as displayed in Fig. 7b at different scan rates from 5 to 40 mV s^{-1}. Fig. 7c illustrates the galvanostatic discharge curves of the ASC device at different current densities. The device reached an ultrahigh specific capacitance of 112.4 F g^{-1} at a high current density of 5 A g^{-1} based on the total mass of positive and negative electrode active materials. The long-term cycling performance of the ASC device was tested by galvanostatic charge and discharge processes at 5 A g^{-1}. As shown in Fig. 7d, the ASC device possesses an excellent cycling stability with approximately 99% of specific capacitance retention after 10000 cycles and a high Coulombic efficiency.

The energy density and power density are two crucial characteristics for hybrid capacitors. Fig. 7e compares the Ragone plot of the ASC device with other reports [23,25,26,44–46]. Remarkably, the ASC device we assembled achieved an ultrahigh energy density of 50.56 Wh kg^{-1} at a power density of 4.6 kW kg^{-1}, and retained 20.93 Wh kg^{-1} at a high power density of 22.5 kW kg^{-1}. These results are better than those of ASC devices reported previously, such as $CuCo_2S_4$//AC (15.6 Wh kg^{-1} at 3.0 kW kg^{-1}) [23], $CuCo_2S_4$ NRAs//AC (26.29 Wh kg^{-1} at 4.8 kW kg^{-1}) [44], $CuCo_2S_4$/NG//AC (47.5 Wh kg^{-1} at 4 kW kg^{-1}) [45], $CuCo_2S_4$-HNN//AC (44.1 Wh kg^{-1} at 0.8 kW kg^{-1}) [25], $CuCo_2S_4$//AC (35.15 Wh kg^{-1} at 6.64 kW kg^{-1}) [46] and $CuCo_2S_4$//AC (31.88 Wh kg^{-1} at 3.02 kW kg^{-1}) [26]. Finally, two ASC devices which were connected in series were able to power a LED light (3 V) for a long time after being charged due to the high energy density of ASC devices, as shown in Fig. 7f.

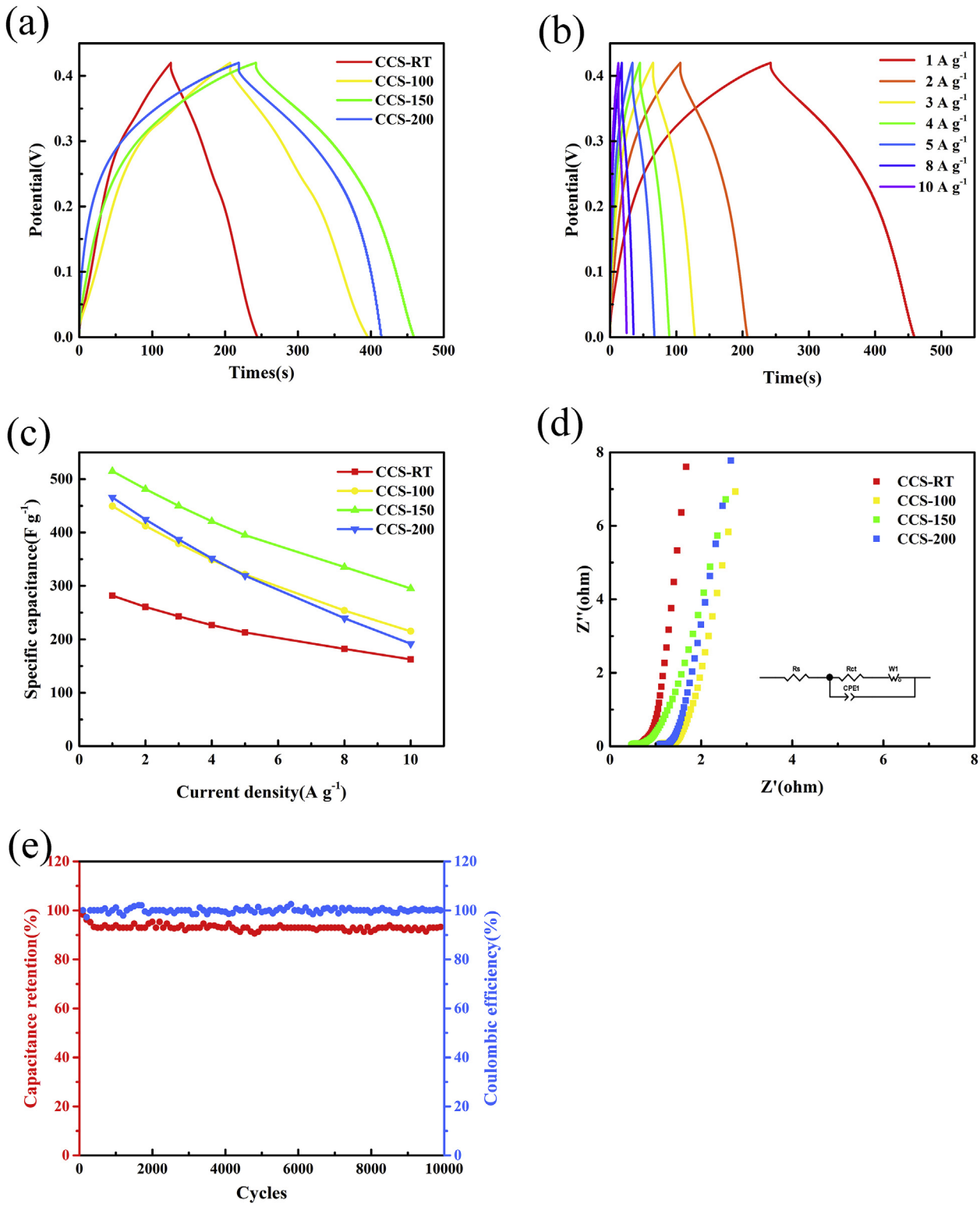

Fig. 6. (a) Galvanostatic charge and discharge curves of $CuCo_2S_4$ electrodes at 1 A g^{-1}, (b) galvanostatic charge and discharge curves of CCS-150 electrode at various current densities, (c) dependence of specific capacitance of $CuCo_2S_4$ electrodes on current density, (d) EIS Nyquist plots of $CuCo_2S_4$ electrodes and (e) cycling performance of CCS-150 electrode at 5 A g^{-1}.

4. Conclusions

$CuCo_2S_4$ materials have been successfully synthesized by a simple hydrothermal method using Cu-Co carbonate hydroxide as the precursor in Na_2S solution. The Cu-Co precursor would go through an amorphous-crystalline transition during the sulfidation and hydrothermal process, and the reaction temperature was a crucial factor to the crystallinity, morphology and electrochemical

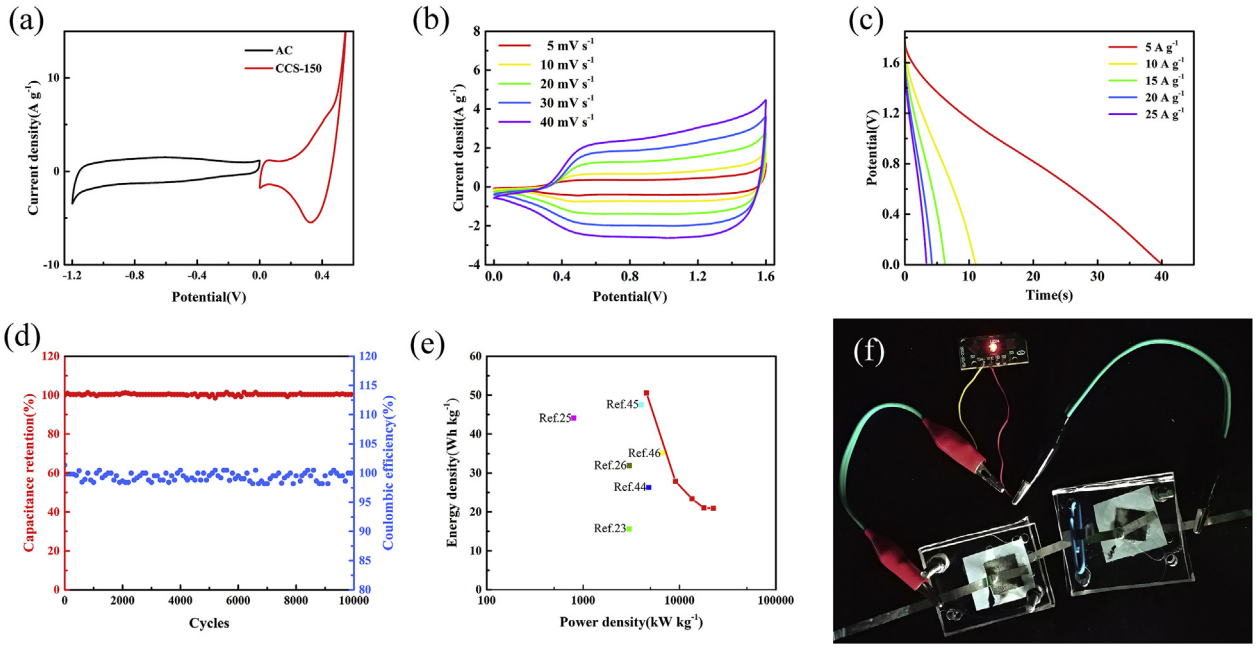

Fig. 7. Electrochemical performances of hybrid capacitor, (a) CV curves of positive and negative electrodes at a scan rate of 5 mV s^{-1}, (b) CV curves at different scan rates within 1.6 V, (c) galvanostatic discharge curves at various current densities, (d) cycling performances of the device at 5 A g^{-1}, (e) Ragone plot and (f) photograph of a commercial LED in red color powered by two ASC devices connected in series. (For interpretation of the references to color in this figure legend, the reader is referred to the Web version of this article.)

performances of $CuCo_2S_4$ materials. The optimized CCS-150 electrode was able to exhibit a specific capacitance of 515 F g^{-1} at 1 A g^{-1} and good cycling stability of 93.3% retention after 10000 cycles. Meanwhile, the assembled ASC device had an ultrahigh energy density of 50.56 Wh kg^{-1} at a power density of 4.6 kW kg^{-1} and an excellent cycling stability with ~99% retention after 10000 cycles. These above results demonstrate that the as-synthesized $CuCo_2S_4$ materials are of practical application for energy storage.

Acknowledgement

This work was financially supported by Zhejiang Provincial Natural Science Foundation of China (No. LY18E020003) and Fundamental Research Funds for the Central Universities (lzujbky-2016-114).

Appendix A. Supplementary data

Supplementary data related to this article can be found at https://doi.org/10.1016/j.electacta.2018.03.189.

References

[1] Q. Wang, D. Chen, D. Zhang, Electrospun porous $CuCo_2O_4$ nanowire network electrode for asymmetric supercapacitors, RSC Adv. 5 (2015) 96448–96454.
[2] D. Guo, L. Lai, A. Cao, H. Liu, S. Dou, J. Ma, Nanoarrays: design, preparation and supercapacitor applications, RSC Adv. 5 (2015) 55856–55869.
[3] X. Duan, J. Xu, Z. Wei, J. Ma, S. Guo, H. Liu, S. Dou, Atomically thin transition-metal dichalcogenides for electrocatalysis and energy storage, Small Methods 1 (2017), 1700156.
[4] X. Deng, Z. Wei, C. Cui, Q. Liu, C. Wang, J. Ma, Oxygen-deficient anatase TiO_2@C nanospindles with pseudocapacitive contribution for enhancing lithium storage, J. Mater. Chem.A 6 (2018) 4013–4022.
[5] C. Cui, J. Xu, L. Wang, D. Guo, M. Mao, J. Ma, T. Wang, Growth of $NiCo_2O_4$@$MnMoO_4$ nanocolumn arrays with superior pseudocapacitor properties, ACS Appl. Mater. Interfaces 8 (2016) 8568–8575.
[6] K. Ma, J.P. Cheng, J. Zhang, M. Li, F. Liu, X. Zhang, Dependence of Co/Fe ratios in Co-Fe layered double hydroxides on the structure and capacitive properties, Electrochim. Acta 198 (2016) 231–240.
[7] T.M. Masikhwa, J.K. Dangbegnon, A. Bello, M.J. Madito, D. Momodu, F. Barzegar, N. Manyala, Effect of growth time of hydrothermally grown cobalt hydroxide carbonate on its supercapacitive performance, J. Phys. Chem. Solids 94 (2016) 17–24.
[8] C. Sheng, Z. Junwu, W. Xin, One-step synthesis of graphene-cobalt hydroxide nanocomposites and their electrochemical properties, J. Phys. Chem. C 114 (2010) 11829–11834.
[9] D. Zhang, M. Han, Y. Li, J. He, B. Wang, K. Wang, H. Feng, Ultra-facile fabrication of phosphorus doped egg-like hierarchic porous carbon with superior supercapacitance performance by microwave irradiation combining with self-activation strategy, J. Power Sources 372 (2017) 260–269.
[10] M. Li, J.P. Cheng, F. Liu, X.B. Zhang, 3D-architectured nickel–cobalt–manganese layered double hydroxide/reduced graphene oxide composite for high-performance supercapacitor, Chem. Phys. Lett. 640 (2015) 5–10.
[11] M. Li, J.P. Cheng, J. Wang, F. Liu, X.B. Zhang, The growth of nickel-manganese and cobalt-manganese layered double hydroxides on reduced graphene oxide for supercapacitor, Electrochim. Acta 206 (2016) 108–115.
[12] S. Chen, W. Ma, H. Xiang, Y. Cheng, S. Yang, W. Weng, M. Zhu, Conductive, tough, hydrophilic poly(vinyl alcohol)/graphene hybrid fibers for wearable supercapacitors, J. Power Sources 319 (2016) 271–280.
[13] J. Zhang, H. Feng, Q. Qin, G. Zhang, Y. Cui, Z. Chai, W. Zheng, Interior design of three-dimensional CuO ordered architectures with enhanced performance for supercapacitors, J. Mater. Chem.A 4 (2016) 6357–6367.
[14] L. Wang, Z.H. Dong, Z.G. Wang, F.X. Zhang, J. Jin, Layered α-$Co(OH)_2$ nanocones as electrode materials for pseudocapacitors: understanding the effect of interlayer space on electrochemical activity, Adv. Funct. Mater. 23 (2013) 2758–2764.
[15] A. Pendashteh, S.E. Moosavifard, M.S. Rahmanifar, Y. Wang, M.F. El-Kady, R.B. Kaner, M.F. Mousavi, Highly ordered mesoporous $CuCo_2O_4$ nanowires, a promising solution for high-performance supercapacitors, Chem. Mater. 27 (2015) 3919–3926.
[16] A. Pendashteh, M.S. Rahmanifar, R.B. Kaner, M.F. Mousavi, Facile synthesis of nanostructured $CuCo_2O_4$ as a novel electrode material for high-rate supercapacitors, Chem. Commun. 50 (2014) 1972–1975.
[17] Y. Luo, J. Luo, W. Zhou, X. Qi, H. Zhang, D.Y.W. Yu, C.M. Li, H.J. Fan, T. Yu, Controlled synthesis of hierarchical graphene-wrapped TiO_2@Co_3O_4coaxial nanobelt arrays for high-performance lithium storage, J. Mater. Chem. A 1 (2013) 273–281.
[18] X. Li, Q. Li, Y. Wu, M. Rui, H. Zeng, Two-Dimensional, porous nickel-cobalt sulfide for high-performance asymmetric supercapacitors, ACS Appl. Mater. Interfaces 7 (2015) 19316–19323.
[19] H. Xie, S. Tang, J. Zhu, S. Vongehr, X. Meng, A high energy density asymmetric all-solid-state supercapacitor based on cobalt carbonate hydroxide nanowire covered N-doped graphene and porous graphene electrodes, J. Mater. Chem. A 3 (2015) 18505–18513.
[20] X. Ji, S. Cheng, L. Yang, Y. Jiang, Z.-j. Jiang, C. Yang, H. Zhang, M. Liu, Phase transition–induced electrochemical performance enhancement of hierarchical $CoCO_3$/CoO nanostructure for pseudocapacitor electrode, Nano Energy 11 (2015) 736–745.

[21] J. Cheng, H. Yan, Y. Lu, K. Qiu, X. Hou, J. Xu, L. Han, X. Liu, J.-K. Kim, Y. Luo, Mesoporous $CuCo_2O_4$ nanograsses as multi-functional electrodes for supercapacitors and electro-catalysts, J. Mater. Chem. A 3 (2015) 9769–9776.
[22] Y. Gao, L. Mi, W. Wei, S. Cui, Z. Zheng, H. Hou, W. Chen, Double metal ions synergistic effect in hierarchical multiple sulfide microflowers for enhanced supercapacitor performance, ACS Appl. Mater. Interfaces 7 (2015) 4311–4319.
[23] Y. Zhang, J. Xu, Y. Zhang, Y. Zheng, X. Hu, Z. Liu, Facile fabrication of flower-like $CuCo_2S_4$ on Ni foam for supercapacitor application, J. Mater. Sci. 52 (2017) 9531–9538.
[24] T. Wang, M. Liu, H. Ma, Facile synthesis of flower-like copper-cobalt sulfide as binder-free faradaic electrodes for supercapacitors with improved electrochemical properties, Nanomaterials (Basel) 7 (2017) 140.
[25] S.E. Moosavifard, S. Fani, M. Rahmanian, Hierarchical CuCo2S4 hollow nanoneedle arrays as novel binder-free electrodes for high-performance asymmetric supercapacitors, Chem. Commun. 52 (2016) 4517–4520.
[26] Y. Wang, D. Yang, T. Zhou, J. Pan, T. Wei, Y. Sun, Oriented $CuCo_2S_4$ nanograss arrays/Ni foam as an electrode for a high-performance all-solid-state supercapacitor, Nanotechnology 28 (2017), 465402.
[27] S.H. Guo, P.W. Yuan, J. Wang, W.Q. Chen, K.Y. Ma, F. Liu, J.P. Cheng, One-step synthesis of copper-cobalt carbonate hydroxide microsphere for electrochemical capacitors with superior stability, J. Electroanal. Chem. 807 (2017) 10–18.
[28] C.S. Dai, P.Y. Chien, J.Y. Lin, S.W. Chou, W.K. Wu, P.H. Li, K.Y. Wu, T.W. Lin, Hierarchically structured Ni_3S_2/carbon nanotube composites as high performance cathode materials for asymmetric supercapacitors, ACS Appl. Mater. Interfaces 5 (2013) 12168–12174.
[29] L. Hu, Y. Deng, K. Liang, X. Liu, W. Hu, $LaNiO_3$/NiO hollow nanofibers with mesoporous wall: a significant improvement in NiO electrodes for supercapacitors, J. Solid State Electrochem. 19 (2015) 629–637.
[30] K. Ma, F. Liu, M. Zhang, X. Zhang, J.P. Cheng, Core/shell microrod arrays of NiO/Co-Fe layered double hydroxides deposited on nickel foam for energy storage and conversion, Electrochim. Acta 225 (2017) 425–434.
[31] J. Shen, J. Tang, P. Dong, Z. Zhang, J. Ji, R. Baines, M. Ye, Construction of three-dimensional $CuCo_2S_4$/CNT/graphene nanocomposite for high performance supercapacitors, RSC Adv. 6 (2016) 13456–13460.
[32] J.A. Dean, Lange's Handbook of Chemistry, McGraw-Hill ed., New York, 1999.
[33] P. Atkins, Physical Chemistry, Eighth ed., 2006. New York.
[34] K. Xu, W. Li, Q. Liu, B. Li, X. Liu, L. An, Z. Chen, R. Zou, J. Hu, Hierarchical mesoporous $NiCo_2O_4$@MnO_2 core–shell nanowire arrays on nickel foam for aqueous asymmetric supercapacitors, J. Mater. Chem.A 2 (2014) 4795.
[35] Z. Lu, W. Zhu, X. Lei, G.R. Williams, D. O'Hare, Z. Chang, X. Sun, X. Duan, High pseudocapacitive cobalt carbonate hydroxide films derived from CoAl layered double hydroxides, Nanoscale 4 (2012) 3640–3643.
[36] S. Gu, Z. Lou, X. Ma, G. Shen, $CuCo_2O_4$ nanowires grown on a Ni wire for high-performance, flexible fiber supercapacitors, ChemElectroChem 2 (2015) 1042–1047.
[37] Q. Wang, X. Liang, D. Yang, D. Zhang, Facile synthesis of novel $CuCo_2S_4$ nanospheres for coaxial fiber supercapacitors, RSC Adv. 7 (2017) 29933–29937.
[38] S. Liu, K.S. Hui, K.N. Hui, V.V. Jadhav, Q.X. Xia, J.M. Yun, Y.R. Cho, R.S. Mane, K.H. Kim, Facile synthesis of microsphere copper cobalt carbonate hydroxides electrode for asymmetric supercapacitor, Electrochim. Acta 188 (2016) 898–908.
[39] L. Wang, H. Yang, T. Shu, X. Chen, Y. Huang, X. Hu, Rational design of three-dimensional hierarchical nanomaterials for asymmetric supercapacitors, ChemElectrochem 4 (2017) 2428–2441.
[40] P. Simon, Y. Gogotsi, Materials for electrochemical capacitors, Nature Mater. 7 (2008) 845–854.
[41] L. Qian, L. Gu, L. Yang, H. Yuan, D. Xiao, Direct growth of $NiCo_2O_4$ nanostructures on conductive substrates with enhanced electrocatalytic activity and stability for methanol oxidation, Nanoscale 5 (2013) 7388–7396.
[42] X. Yu, J. Lu, C. Zhan, R. Lv, Q. Liang, Z.-H. Huang, W. Shen, F. Kang, Synthesis of activated carbon nanospheres with hierarchical porous structure for high volumetric performance supercapacitors, Electrochim. Acta 182 (2015) 908–916.
[43] L.L. Zhang, X.S. Zhao, Carbon-based materials as supercapacitor electrodes, Chem. Soc. Rev. 38 (2009) 2520–2531.
[44] S. Cheng, T. Shi, C. Chen, Y. Zhong, Y. Huang, X. Tao, J. Li, G. Liao, Z. Tang, Construction of porous $CuCo_2S_4$ nanorod arrays via anion exchange for high-performance asymmetric supercapacitor, Sci. Rep. 7 (2017) 6681.
[45] M. Guo, J. Balamurugan, T.D. Thanh, N.H. Kim, J.H. Lee, Facile fabrication of Co_2CuS_4 nanoparticle anchored N-doped graphene for high-performance asymmetric supercapacitors, J. Mater. Chem.A 4 (2016) 17560–17571.
[46] A.T.A. Ahmed, H.S. Chavan, Y. Jo, S. Cho, J. Kim, S.M. Pawar, J.L. Gunjakar, A.I. Inamdar, H. Kim, H. Im, One-step facile route to copper cobalt sulfide electrodes for supercapacitors with high-rate long-cycle life performance, J. Alloys Compds. 724 (2017) 744–751.